Dust Studies in DIII-D and TEXTOR

D.L. Rudakov 1), A. Litnovsky 2), W.P. West 3), J.H. Yu 1), J.A. Boedo 1), B.D. Bray 3), S. Brezinsek 2), N.H. Brooks 3), M.E. Fenstermacher 4), M. Groth 4), E.M. Hollmann 1), A. Huber 2), A.W. Hyatt 3), S.I. Krasheninnikov 1), C.J. Lasnier 4), R.A. Moyer 1), A.Yu. Pigarov 1), V. Philipps 2), A. Pospieszczyk 2), R.D. Smirnov 1), J.P. Sharpe 5), W.M. Solomon 6), J.G. Watkins 7), and C.P.C. Wong 3)

1) University of California, San Diego, La Jolla, California 92093-0417, USA
2) Institut für Energieforschung-Plasmaphysik, Forschungszentrum Jülich, Association EURATOM-FZJ, 52425 Germany
3) General Atomics, P.O. Box 85608, San Diego, California 92186-5608, USA
4) Lawrence Livermore National Laboratory, Livermore, California 94551, USA
5) Idaho National Engineering and Environmental Laboratory, Fusion Safety Program, Idaho Falls, Idaho 83415, USA
6) Princeton Plasma Physics Laboratory, Princeton, New Jersey, USA
7) Sandia National Laboratories, Albuquerque, New Mexico 87185, USA

e-mail contact of main author: rudkov@fusion.gat.com

Abstract. Studies of naturally occurring and artificially introduced carbon dust are conducted in DIII-D and TEXTOR. In DIII-D, dust does not present operational concerns except immediately after entry vents. Energetic plasma disruptions produce significant amounts of dust. However, dust production by disruptions alone is insufficient to account for the estimated in-vessel dust inventory in DIII-D. Submicron sized dust is routinely observed using Mie scattering from a Nd:Yag laser. The source is strongly correlated with the presence of Type I edge localized modes (ELMs). Larger size (0.005-1 mm diameter) dust is observed by optical imaging, showing elevated dust levels after entry vents. Inverse dependence of the dust velocity on the inferred dust size is found from the imaging data. Migration of pre-characterized carbon dust is studied in DIII-D and TEXTOR by injecting micron-size dust in plasma discharges. In DIII-D, a sample holder filled with ~30 mg of dust is introduced in the lower divertor and exposed to high-power ELMing H-mode discharges with strike points swept across the divertor floor. After a brief exposure (~0.1 s) at the outer strike point, part of the dust is injected into the plasma, raising the core carbon density by a factor of 2–3 and resulting in a twofold increase of the radiated power. Individual dust particles are observed moving at velocities of 10–100 m/s, predominantly in the toroidal direction, consistent with the drag force from the deuteron flow and in agreement with modeling by the 3D DustT code. In TEXTOR, instrumented dust holders with 1–45 mg of dust are exposed in the scrape-off layer 0–2 cm radially outside of the last closed flux surface in discharges heated with neutral beam injection (NBI) power of 1.4 MW. Dust is launched either in the beginning of a discharge or at the initiation of NBI, preferentially in a direction perpendicular to the toroidal magnetic field. At the given configuration of the launch, the dust did not penetrate the core plasma and only moderately perturbed the edge plasma, as evidenced by an increase of the edge carbon content.

1. Introduction

Dust is commonly found in magnetic fusion devices [1–8]. In contemporary machines dust is generally of little concern from an operational or safety standpoint. However, dust generation in next-step devices is expected to increase by several orders of magnitude due to the increased duty cycle and higher magnitude of particle and power fluxes deposited on the plasma facing components (PFCs). Dust production and accumulation present potential safety and operational issues for ITER by contributing to tritium inventory rise and leading to radiological and explosion hazards. The total in-vessel dust inventory in ITER will be limited to 1000 kg to ensure that environmental releases stay below the design limits in the case of the worst credible accident. A lower administrative limit of 670 kg has been proposed to take account of measurement uncertainties. The enhanced chemical activity of dust at high

temperatures is more restrictive, since in the case of an in-vessel coolant leak hot Be and C dust can react with steam/water causing hydrogen generation and (in the case of simultaneous air ingress) explosion hazard. Thus a limit of 11 kg for Be and 15 kg for C dust on hot surfaces is being considered. More projections of dust production and accumulation rates based on experience from existing tokamaks and disruption simulators are needed. In addition, dust penetration of the core plasma can cause undesirably high impurity concentration and degrade performance. Thus, studies of the dust transport and dynamics are also quite important. Here we report studies of naturally occurring and artificially introduced dust in DIII-D and TEXTOR.

2. Studies of Naturally Occurring Dust in DIII-D

Dust particulates found in tokamaks range in size between ~10 nm and a few hundred μm [1,3–8]. Chemical composition of dust is determined mainly by the PFC materials; hence, in tokamaks with carbon-based PFCs, such as DIII-D and TEXTOR, dust is mostly carbon, though it may contain plasma fuel elements and impurities. Dust production mechanisms include flaking of redeposited layers, brittle destruction of graphite, arcing, agglomeration from supersaturated vapor, and growth from hydrocarbon molecules [6]. Additionally, disruptions, edge localized modes (ELMs) and other transient events result in increased dust production.

Dust collection has been performed in DIII-D during entry vents [3]. The median diameters of the collected dust samples ranged between 0.46 and 1.0 μm. The total in-vessel dust inventory was estimated to be between 33–120 g [3].

During plasma operations on DIII-D, dust is present in the scrape-off layer (SOL) and edge plasma, but it does not appear to present any problem. Evidence of the dust presence comes from a few diagnostics, including Mie scattering from ND:YAG lasers, visible imaging and survey spectroscopy. A Thomson scattering system based on 8 Nd:YAG lasers is used primarily for the measurements of the electron density and temperature profiles. Each laser produces pulses of about 10 ns duration at a 20 Hz repetition rate with a total energy per pulse of 0.5 J. The vertical core system has four collinear lasers, while the divertor system has a single laser. The laser beam has a center region of high intensity (above 10^{12} Wm^{-2}) 3 mm in diameter, surrounded by a halo region with about 5% of the center intensity that extends out to a diameter of 5 mm [9]. Light scattered from multiple positions along the laser path inside the plasma is collected by an optical system located outside the vacuum vessel and directed to polychromators, each with 6 detectors at different wavelengths. Viewing volumes are typically 1 cm in height and 5 mm in diameter. Non-shifted detector channels at the laser wavelength of 1064 nm allow for detection of light scattered by the dust particles. Signals from large particles cause saturation of the non-shifted channels, but some of them can be resolved by detectors with narrow band filters centered at 1062 nm which have an extinction factor ~10^{-2} at the laser wavelength. More detail on dust detection by the Thomson scattering system is available in Ref. [9].

Because of the short laser pulse duration and small viewing volume, dust observation rates are low, only a few events per discharge or less. Nevertheless, statistical analysis of the data provides an estimate of the total dust content in the edge and SOL plasmas, and allows establishing trends in dust production rates. Dust size can be estimated from the amplitude of the scattered signal detected. An analysis using a Mie scattering model and taking particle ablation by the laser into account has put the detectable particle size within the range of 0.16–1.6 μm in diameter [10]. Probability distribution functions (PDFs) of the radii of experimentally detected dust particles are shown in Fig. 1(a). The PDFs were constructed from a fit to the scattering signal distribution obtained over 710 discharges comprising 1580

dust events [9] assuming graphite particles with complex index of refraction m = 3.33-i2.07 [10]. The dashed line is obtained assuming the detected particles were in the center region of the beam, and the solid line is obtained assuming the particles were in the halo region. For smaller particles (R < 0.2 μm), the slope of the PDF is close to R^{-3}, while for larger particles it is smaller. Therefore, the contribution of large particles to the total dust mass is larger than that of small ones despite the much larger number density of small particles. Figure 1(b) shows measured dust density profiles in low confinement (L-) and high confinement (H-) modes. The dust density is near the detection limit at the last closed flux surface (LCFS) and increases with distance into the SOL. It is higher in H-mode that has higher heating power and ELMs causing more intense plasma-wall interaction. Correlation of increased dust production with the presence of large ELMs has been established [11,12]. Dust density increases with increasing ELM amplitude compared to discharges with similar stored energy and more frequent smaller ELMs [12]. However, even at the highest dust densities measured and with the dust size determined using Mie model, estimated total carbon content of the dust is less than a few percent of the plasma carbon impurity content. Based on this result, we conclude that submicron dust is not a major impurity source in DIII-D.

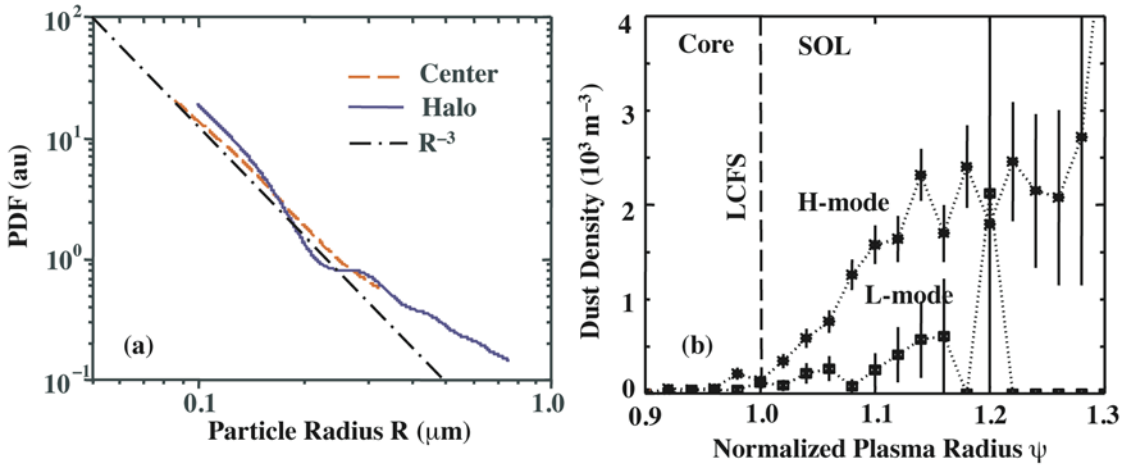

FIG. 1. Dust size distribution (a) and radial density profile (b) measured by Mie scattering.

Larger dust particles are detected by optical imaging with cameras. A number of standard frame rate CMOS and CID cameras and a fast framing CMOS camera are available on DIII-D. A tangential view of the lower divertor is split between two standard rate (60 images/s) CID cameras ("tangential TVs"). Spatial resolution of both tangential TVs is about 1.5–2.0 cm. A standard rate CMOS camera ("DiMES TV") views vertically down into the lower divertor with a spatial resolution of about 1.5 mm. A fast framing (up to 26000 images/s) CMOS camera (Phantom 7.1) [13] has a tangential view of the outboard chamber wall with a spatial resolution of about 5 mm. Since the fast camera has an inherently higher contrast ratio for moving incandescent objects than the standard rate cameras, it can resolve smaller particles, so the dust observation rate using the fast camera is much higher than that of the standard cameras.

During "normal operations", i.e., when the vacuum vessel walls are well conditioned and there are no major disruptions, standard cameras register only isolated dust events in their field of view (typically single digit numbers per discharge or less) while the fast camera typically observes between 10–100 events per discharge. Individual particles move at velocities of up to ~500 m/s. Breakup of larger particles into pieces is sometimes observed. A sequence of frames in Fig. 2 shows a comparatively large and slow (probably tens of microns in size and ~10 m/s in velocity) dust particle marked by an arrow in (a) that first becomes

visible in the outboard SOL. Though reconstruction of the exact trajectory from a 2D image is impossible, it appears that the particle first moves towards the LCFS (b), then slows down (c), changes direction (d), and finally breaks into three smaller particles (e–h). These data were taken by the fast camera without a filter, at 2000 frames/s. The total time between frames (a) and (h) is ~60 ms, and time between individual frames varies between 8–10 ms.

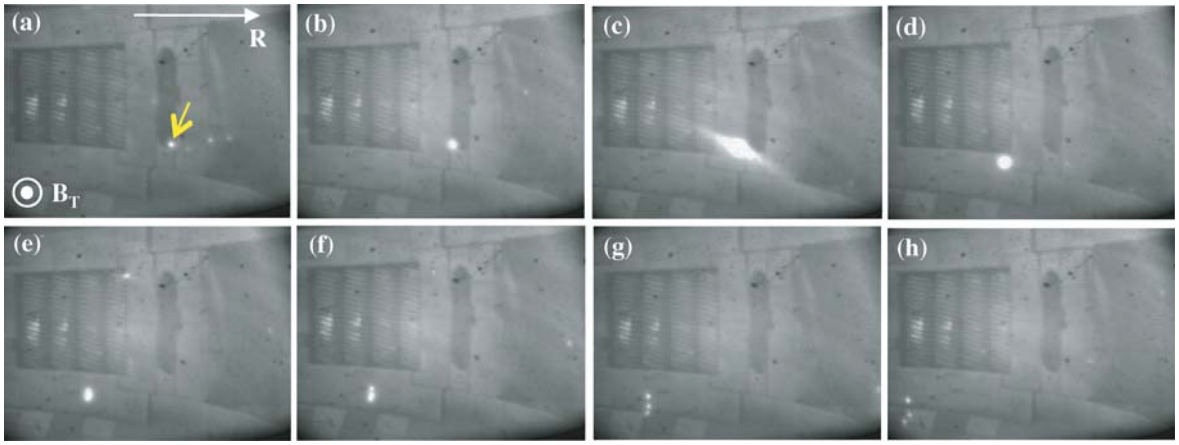

FIG. 2. Time history of a dust particle observed by the fast camera in the outboard DIII-D SOL.

Disruptions often generate significant amounts of dust which is directly observed by the fast-framing camera. A raw image of dust produced by a disruption with an upward-going vertical displacement event (VDE) is shown in Fig. 3(a). Figure 3(b) shows dust trajectories traced for ~8 ms after a similar disruption. The median velocity of these particles is 100 m/s, and particles with velocities as high as 280 m/s are observed. A disruption produces up to ~1000 dust particles within the camera view, corresponding to ~10000 particles for the whole vessel. This corresponds to between 0.01–1 mg of carbon, depending on the dust size which is hard to determine from the camera data. Taking the upper bound estimate, disruptions in DIII-D may produce up to ~1 g of dust over a 15 week experimental campaign. This is two orders of magnitude below the estimated in-vessel dust inventory [3], so other mechanisms are likely to dominate the dust production. It is possible that a large part of the dust inventory in DIII-D is created by in-vessel activities during vents. In the first 2–3 plasma discharges after an entry vent, standard rate cameras detect hundreds of particles and the fast camera detects thousands of particles in each discharge. An example of dust tracks observed by DiMES TV viewing the lower divertor from above is shown in Fig. 3(c). After about 15 discharges dust is virtually gone during the stationary portion of a discharge, and appears at much reduced levels during the plasma initiation and termination phases. After a few days of plasma operations (about 70 discharges) dust levels are further reduced to the "normal operations" rates.

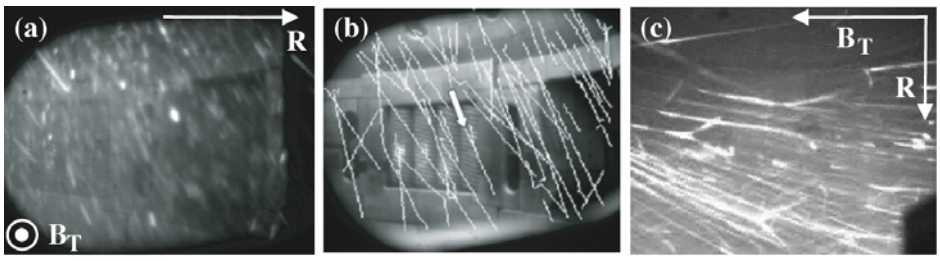

FIG. 3. (a) Image of dust produced by a disruption with upward VDE (fast camera, tangential view of the outboard SOL); (b) dust trajectories traced for ~8 ms after a similar disruption; (c) dust observed after an entry vent (DiMES TV, looking down in the divertor).

In principle, if chemical composition and the local plasma parameters at the location of a dust particle are known, one can relate the intensity of thermal radiation from a particle to the particle size [7,14]. If an absolute *in situ* calibration of the camera sensitivity is available, it may be possible to determine the particle size from the intensity of a recorded image, however, in practice this task is extremely complicated. Luminosity of a dust particle is a very strong function of the local plasma density, n_e, and electron temperature, T_e [7,14]. Since gradients of n_e and T_e with typical e-folding lengths of 2–8 cm exist in the SOL [15], with a 2D view it's practically impossible to determine a particle position with sufficient accuracy for a reasonable size estimate. In addition, line radiation from the ablation cloud around a particle can contribute significantly to or even dominate the detected radiation [Fig. 2(c)]. An alternative approach for determination of a particle size from camera data involves comparison of a particle life time in the plasma with a theoretical ablation rate of a carbon sphere [14]. This method has been recently applied in DIII-D [16]. Life times of the dust particles ablated by ELM filaments propagating outwards across the outboard SOL were measured from the fast camera images. Plasma parameters inside the ELM filaments were assumed to be comparable to those at the top of H-mode edge pedestal (typically $n_{e,ped}$ = $3x10^{13}$ cm^{-3} and $T_{e,ped}$ = 400 eV). Most dust particles are destroyed within a single ELM, however, the largest observed particles survive up to 12 ELMs. A distribution of inferred dust size was constructed based on 2,330 particles detected by the fast camera during H-mode operation in 12 plasma discharges [16]. The inferred particle diameters were between ~3 mm and ~1 mm. The upper end, however, may be an overestimate, since the decay of the density and temperature inside ELM filaments propagating through the SOL was neglected, so the ablation rates were probably overestimated.

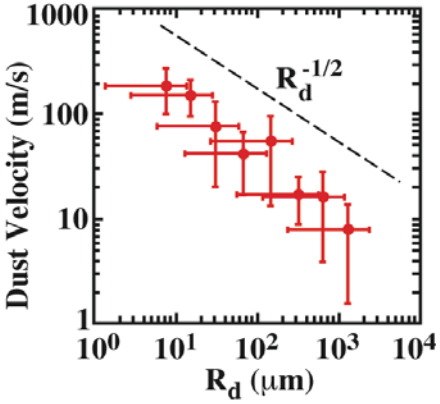

FIG. 4. Measured 2D dust velocity decreases with the dust size inferred from the ablation model.

Correlation of the dust velocity with the inferred dust size has been studied [16]. From the camera data it's only possible to measure a 2D velocity projection onto a plane perpendicular to the viewing direction, which is a lower limit on actual 3D velocity magnitude. Figure 4 shows the projected velocities versus the inferred particle radii. The vertical bars represent the standard deviation of velocities for particles in each radius bin. The horizontal bars show variation in the inferred radius when n_e and T_e are varied by a factor of 2 from the pedestal values. An inverse dependence with a slope close to $R_d^{-1/2}$ (dashed line shown for comparison in Fig. 4) has been found. This is consistent with modeling by the DustT code [17], which predicts that smaller particles experience faster acceleration by the ion drag force. The $R_d^{-1/2}$ scaling of the dust velocity is also predicted by a simplified one-dimensional uniform plasma model [17].

3. Experiments with Intentionally Introduced Dust in DIII-D and TEXTOR

Injections of pre-characterized dust from a known location can be used to calibrate diagnostic measurements and benchmark modeling of dust dynamics and transport. Migration of carbon dust has been studied in DIII-D by introduction of micron-size (0.8–15 μm diameter with a median of ~6 μm) graphite dust in the lower divertor [18]. A series of experiments was performed. In each case, 25–40 mg of dust was placed on a graphite Divertor Material Evaluation System (DiMES) sample holder and inserted in the lower divertor flush with the tile surface. The dust was then exposed to ELMing H-mode discharges with strike points

swept across the divertor floor. The typical discharge parameters were: toroidal magnetic field, B_T = 2 – 2.1 T, plasma current, I_p = 1.1 – 1.4 MA, neutral beam injection (NBI) heating power, P_{NBI} = 4.5–8.5 MW, line-average plasma density, $\bar{n}_e$ = 4.5 – 6.0x10^{19} m^{-3}. In the early part of the discharge the holder with dust was kept in the private flux region (as shown in Fig. 5(a), black separatrix), then the outer strike point (OSP) was swept radially inward over the dust. Following a brief exposure (~0.1 s) at the OSP, part of the dust was injected into the plasma. A frame from the tangential divertor TV with infrared filter shows a direct view of the injection [Fig. 5(c), the DiMES location is marked by a circle]. About 1.5%–2.0% of the total dust carbon content (2–3×10^{19} carbon atoms, equivalent to a few million dust particles) penetrated the core plasma, raising the core carbon density by a factor of 2–3 and resulting in a twofold increase of the total radiated power [Fig. 5(b)]. Individual dust particles were observed moving at velocities of 10–100 m/s, predominantly in the toroidal direction for deuteron flow towards the outer divertor target (which in these experiments was in the direction of B_T), consistent with the ion drag force. Observed velocities and trajectories of the dust particles are in qualitative agreement with modeling by the DustT code [7,14,17]. The fast framing camera observed large amounts of injected dust in the outboard SOL [Fig. 5(d)], thus confirming the DustT prediction that dust can migrate from the lower divertor into the main chamber [14]. An injection of diamond dust of finely calibrated size between 2 – 4 microns was recently performed. Dust from injection was observed by the fast camera, but required digital background subtraction to be resolved. Therefore, it was experimentally demonstrated that 4 micron dust is about the smallest that can be resolved by the fast camera in the existing setup at DIII-D.

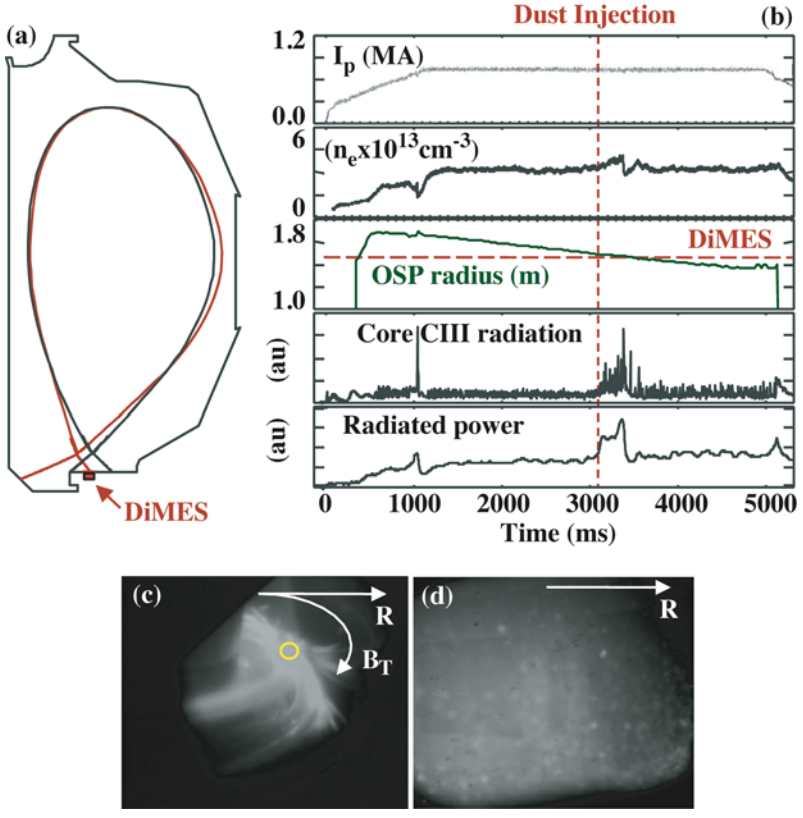

FIG. 5. Dust experiments in DIII-D: (a) dust exposure geometry; (b) temporal evolution of the discharge and plasma parameters; (c) dust injection observed by the tangential divertor TV; (d) injected dust observed in the outboard SOL by the fast framing camera.

Dedicated experiments with dust have started recently in TEXTOR. Pre-characterized carbon dust similar to that used in DIII-D [18] was introduced in amounts ranging from 1 to

45 mg on instrumented dust holders. The holders were mounted on the spherical test-limiter and exposed one by one in the SOL of TEXTOR using the Limiter Lock transport system at the bottom of the vacuum vessel. The view of the limiter with a dust holder is shown in Fig. 6(a). Three holders with different amounts of dust were exposed during repetitive NBI-heated discharges with P_{NBI} = 1.4 MW and $\bar{n}_e$ = 2.5×10^{19} m^{-3}, at the radial locations from 0 to 2 cm outside of the LCFS. Local plasma parameters near the dust launch locations were $n_{e.loc}$ ~ 2–2.5×10^{18} m^{-3} and $T_{e.loc}$ ~ 30–35 eV. During the exposure of instrumented holders the dust launch occurred either in the beginning of the discharge at t = 0 s or at t = 1.5 s when NBI injector was activated. Analyses of recorded video sequences from a downward-looking camera without a filter [Fig. 6(b)] evidenced the launch of dust in a direction perpendicular to the toroidal magnetic field. The motion of the dust was caused by the Lorentz force due to the thermoelectron current emitted by the hot dust particles in the same way as it was earlier observed in TEXTOR during experiments with tungsten melt layer formation [19].

An extensive set of plasma diagnostics was used to investigate the motion of the dust in TEXTOR plasmas and its impact on the core performance. The diagnostics involved the Thomson scattering system, operating both in active and in passive (without laser irradiation) modes, fast cameras and a set of edge and core spectroscopes including the high efficiency extreme ultraviolet overview spectrometer system HEXOS [20]. After exposure of the dust samples, careful analysis of the data from the core spectroscopy systems, fast cameras and Thomson scattering system did not reveal any measurable change of the core performance.

The amount of dust launched during TEXTOR discharges was estimated by weighting the dust holders with and without dust before and after the exposures. In the 4 discharges where the dust launch occurred, the total amount of dust lost from the holders was about 43 mg, which corresponds to ~2.2×10^{21} carbon atoms. Given the fact that the detection limit of the core diagnostics is about 10^{13} particles, the conclusion can be made that the dust didn't enter the core of TEXTOR.

At the same time, analyses of the data from edge spectroscopy did reveal clear signals resulting from the dust launch. A 2D image recorded by a horizontally-looking camera equipped with CIII filter is shown in Fig. 6(c). This picture was made during discharge 106265 at a time t = 1510 ms, i.e. immediately after the NBI start. Analysis of the edge spectroscopic data showed that the carbon concentration in edge plasmas increased from around 3% to up to about 6% during the launching events. This increase corresponds to ~10^{17} additional carbon atoms in the edge plasma. Therefore, less than 0.01% of the launched dust carbon content ended up in the plasma. The present understanding is that the major part of the injected dust was deposited on the adjacent PFC surfaces immediately after the launch.

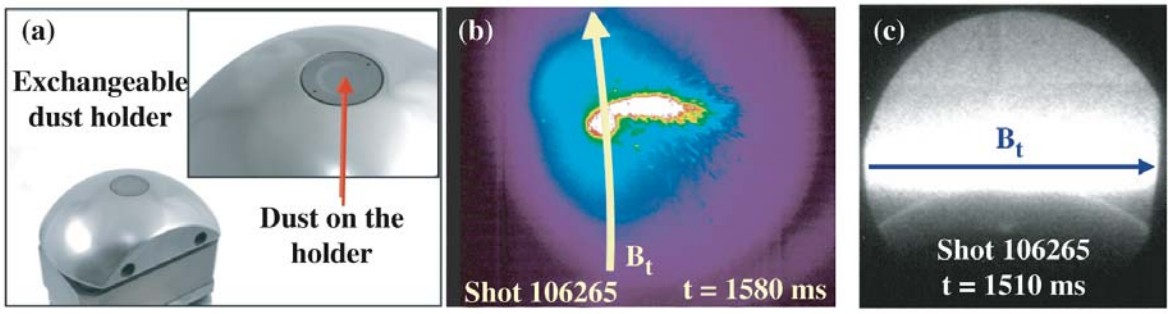

FIG. 6. Dust experiment in TEXTOR: (a) spherical graphite test limiter with exchangeable holder and dust; (b) the launch of dust at the beginning of NBI phase (c) spectroscopic view of the dust launch.

4. Summary and Conclusion

In summary, progress has been made in characterization of naturally occurring and artificially introduced carbon dust in DIII-D and TEXTOR. Micron size dust has been shown to be highly mobile, travelling at velocities of up to hundreds of m/s. Dust does not present operational concerns in DIII-D except immediately after entry vents. Disruptions produce notable amounts of dust, but dust production by disruptions alone is insufficient to account for the estimated in-vessel dust inventory in DIII-D. ELMs are also observed to produce dust in DIII-D. These impulsive sources of dust remain a concern for ITER, where wall loads from ELMs and disruptions will be large compared to those on DIII-D. Experiments with artificially introduced dust in DIII-D showed that dust can migrate from the lower divertor into the main chamber and contribute to the core plasma contamination with impurities. In contrast, the first experiment with artificially introduced dust in TEXTOR demonstrated that, at the given configuration of the launch, the dust did not penetrate the core plasma and only moderately perturbed the edge plasma, as evidenced by a moderate increase of the edge carbon content.

Acknowledgments

This work was supported in part by the US Department of Energy under DE-FG02-07ER54917, DE-FC02-04ER54698, DE-AC52-07NA27344, DE-AC02-76CH03073, and DE-AC04-94AL85000.

References

[1] BEHRISCH, R., *et al.,* J. Nucl. Mater. **76–77**, 437 (1978).
[2] GOODALL, D.H.J., J. Nucl. Mater. **111–112**, 11 (1982).
[3] CARMACK, W.J., *et al.,* Fusion Eng. Des. **39–40**, 477 (1998); CARMACK, W.J., *et al.,* Fusion Eng. Design **51–52**, 477 (2000).
[4] RUBEL, M., *et al.,* Nucl. Fusion **41**, 1087 (2001).
[5] FEDERICI, G., *et al.,* Nucl. Fusion **41**, 1967 (2001).
[6] WINTER, J., Plasma Phys. Control. Fusion **46**, B583 (2004).
[7] PIGAROV, A.Yu., *et al.,* Phys. Plasmas **12**, 122508 (2005).
[8] WANG, Z., *et al., Proc. 2007 ICTP Summer College on Plasma Physics – New Aspects of Plasma Physics*, P. K. Shukla, L. Stenflo, and B. Eliasson (Ed.) (World Scientific, Singapore 2008) pp. 394–475.
[9] WEST, W.P., *et al.,* Plasma Phys. Control. Fusion **48**, 1661 (2006).
[10] SMIRNOV, R.D., *et al.,* Phys. Plasmas **14**, 112507 (2007).
[11] WEST, W.P., BRAY, B.D., J. Nucl. Mater. **363–365**, 107 (2007).
[12] BRAY, B.D., *et al., Proc. 18th Plasma Surface Interactions Conf.,* Toledo, 2008; also "Correlation of submicron dust production in DIII-D to impulsive wall heating from ELMs," submitted to J. Nucl. Mater.
[13] YU, J.H., *et al.,* Phys. Plasmas **15**, 032504 (2008).
[14] SMIRNOV, R.D., *et al.,* Plasma Phys. Control. Fusion **49**, 347 (2007).
[15] RUDAKOV, D.L., *et al.,* Nucl. Fusion **45**, 1589 (2005).
[16] YU, J.H., *et al., Proc. 18th Plasma Surface Interactions Conf.,* Toledo, 2008; also "Fast camera imaging of dust in the DIII-D tokamak," submitted to J. Nucl. Mater.
[17] SMIRNOV, R.D., *et al., Proc. 18th Plasma Surface Interactions Conf.,* Toledo, 2008; also "Modeling of velocity distributions of dust in tokamak edge plasmas and dust-wall collisions," submitted to J. Nucl. Mater.
[18] RUDAKOV, D.L., *et al.,* J. Nucl. Mater. **363–365**, 227 (2007).
[19] SERGIENKO, G., *et al.,* J. Nucl. Mater. **363–365**, 96 (2007).
[20] BIEL, W., *et al.,* Rev. Sci. Instrum. **77**, 10F305 (2006).